

# Estimates of power plant NO<sub>x</sub> emissions and lifetimes from OMI NO<sub>2</sub> satellite retrievals



Benjamin de Foy<sup>a,\*</sup>, Zifeng Lu<sup>b</sup>, David G. Streets<sup>b</sup>, Lok N. Lamsal<sup>c</sup>, Bryan N. Duncan<sup>c</sup>

<sup>a</sup> Department of Earth and Atmospheric Sciences, Saint Louis University, St. Louis, MO, USA

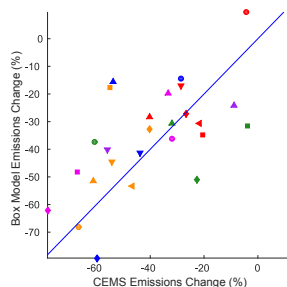
<sup>b</sup> Energy Systems Division, Argonne National Laboratory, Argonne, IL, USA

<sup>c</sup> Atmospheric Chemistry and Dynamics Laboratory, NASA Goddard Space Flight Center, Greenbelt, MD, USA

## HIGHLIGHTS

- Accurate estimations of power plant NO<sub>x</sub> emissions can be made with OMI data.
- Exponentially-Modified Gaussian fit needs multi-annual OMI averages.
- Box Model fit requires seasonal OMI averages for accurate estimates.
- Lifetimes are dominated by a mixed lifetime that does not represent chemical lifetime.
- Continuous Emission Monitoring System (CEMS) provides an excellent emissions test bed.

## GRAPHICAL ABSTRACT



## ARTICLE INFO

### Article history:

Received 13 January 2015

Received in revised form

20 May 2015

Accepted 26 May 2015

Available online 5 June 2015

### Keywords:

Emission inventory

Satellite retrieval

OMI

CEMS

Power plant NO<sub>x</sub>

Chemical lifetime

## ABSTRACT

Isolated power plants with well characterized emissions serve as an ideal test case of methods to estimate emissions using satellite data. In this study we evaluate the Exponentially-Modified Gaussian (EMG) method and the box model method based on mass balance for estimating known NO<sub>x</sub> emissions from satellite retrievals made by the Ozone Monitoring Instrument (OMI). We consider 29 power plants in the USA which have large NO<sub>x</sub> plumes that do not overlap with other sources and which have emissions data from the Continuous Emission Monitoring System (CEMS). This enables us to identify constraints required by the methods, such as which wind data to use and how to calculate background values. We found that the lifetimes estimated by the methods are too short to be representative of the chemical lifetime. Instead, we introduce a separate lifetime parameter to account for the discrepancy between estimates using real data and those that theory would predict. In terms of emissions, the EMG method required averages from multiple years to give accurate results, whereas the box model method gave accurate results for individual ozone seasons.

© 2015 Elsevier Ltd. All rights reserved.

## 1. Introduction

Satellite instruments are increasingly being used as tools for air quality management (Duncan et al., 2014) thanks to their extensive

remote sensing capabilities of atmospheric constituents (Martin, 2008; Hoff and Christopher, 2009). New generations of instruments have made finer resolution measurements such that it is now possible to detect emissions of individual sources (Streets et al., 2013, 2014). Future missions such as TEMPO (Hilsenrath and Chance, 2013), TROPOMI (Veefkind et al., 2012), the Geostationary Environment Monitoring Spectrometer from the Korea

\* Corresponding author.

E-mail address: [bdefoy@slu.edu](mailto:bdefoy@slu.edu) (B. de Foy).

Aerospace Research Institute, and GEO-CAPE (Fishman et al., 2012) will further expand the ability of space-based remote sensing to provide quantitative information on pollution sources. In this paper we use data from the Ozone Monitoring Instrument (OMI, Levelt et al. (2006)) to estimate sources of nitrogen oxides ( $\text{NO}_x = \text{NO}_2 + \text{NO}$ ) from isolated power plants in the USA.

Nitrogen dioxide ( $\text{NO}_2$ ) columns have been validated to  $\pm 25\%$  or better suggesting that mass is fairly accurately known (Bucsele et al., 2008; Boersma et al., 2008; Russell et al., 2011). Decreasing trends of  $\text{NO}_2$  columns over power plants were reported using satellite data by (Kim et al., 2006, 2009). Further analysis of the column data identified the impact of regulations and of the economic recession on both power plant and urban emissions (Russell et al., 2012). More specific constraints on emissions have been obtained by combining the analysis of column retrievals with regional numerical models. For example, Mijling and van der A (2012) used a Kalman filter approach to estimate emissions over China, and Schaap et al. (2013) used a chemical transport model to assess changes in emissions over Europe.

In addition to emissions, satellite column data have been used to obtain information on the chemical lifetimes of  $\text{NO}_2$ , which is a limiting factor in inverting  $\text{NO}_x$  emissions. Mijling and van der A (2012), cited above, obtain  $\text{NO}_x$  lifetimes in Chinese urban areas varying from 3 h in the summer up to 13 h in the winter. Jena et al. (2014) estimated a chemical  $\text{NO}_x$  lifetime of around 10 h based on urban  $\text{NO}_2$  transport off the coast of India. Stavrou et al. (2013) used a model combined with OMI data to examine chemical sinks of  $\text{NO}_x$  in addition to uncertainties in emissions. Valin et al. (2013) identified varying lifetimes as a function of OH concentrations over Riyadh. Valin et al. (2014) further considered the role of OH in spatial differences in weekday-weekend effects in the Los Angeles basin.

In comparison there have been fewer studies estimating emissions directly from the satellite column data without the use of a regional model. Fioletov et al. (2011) used a two-dimensional gaussian fit model with empirically-derived parameters to determine  $\text{SO}_2$  emissions of power plants in the Ohio River Valley. This was used for a variety of large point sources (Fioletov et al., 2013) and for  $\text{SO}_2$  emissions in India (Lu et al., 2013).

Beirle et al. (2011) used the Exponentially-Modified Gaussian (EMG) method to estimate the emissions from Riyadh along with the  $\text{NO}_x$  lifetime. Valin et al. (2013) expanded this method by introducing plume rotation in order to refine the chemical lifetime analysis. The method was also used to estimate volcanic emissions in Hawaii (Beirle et al., 2014) and ship emissions in the Baltic Sea (Ialongo et al., 2014).

A simpler method is to use a mass balance box model. This requires a parameter to relate the column densities to emission rates which is inversely proportional to the residence time of the pollutant in the box. This parameter can be obtained from chemical transport models, as was done for example by Martin et al. (2003); Lee et al. (2011a); Lu and Streets (2012); Ghude et al. (2013); Lamsal et al. (2010); Schaub et al. (2007). Alternatively, Duncan et al. (2013) takes known emissions from US power plants to look at the relationship between changes in emissions and changes in  $\text{NO}_2$  columns. Although OMI could clearly identify reductions in power plant emissions, there was a large scatter in the response parameter between the changes in emissions and the changes in column densities.

de Foy et al. (2014) tested the different estimation methods with synthetic data from the CAMx regional model. They found that the EMG method could give reliable estimates when the plumes were accurately rotated to always be vented in the same direction as suggested by Valin et al. (2013). However, the lifetime estimates

were found to be biased low compared to the true lifetimes in the model simulations. Instead of using the box model method with a parameter derived from simulations, de Foy et al. (2014) derived the parameter from meteorological data in order to obtain emissions estimates directly. The box model method was found to be more robust at estimating emissions than the EMG method, but was dependent on an accurate estimate of the plume speed and of the chemical lifetime.

In this paper we seek to use two of the methods evaluated in de Foy et al. (2014) to refine the response relationship between OMI data and emissions measurements identified in Duncan et al. (2013). We use the Exponentially-Modified Gaussian method and the box model method to determine  $\text{NO}_x$  emissions from power plants and evaluate the results by comparing with data from the Continuous Emissions Monitoring System. We also evaluate the lifetimes obtained from these methods. In Sec. 2 we present the satellite data, the emissions data, the meteorological data, and the estimation methods that we use. The results will be presented for the EMG method and the box model method in Secs. 3.1 and 3.2. We will then show comparisons of the three OMI  $\text{NO}_2$  data products in Sec. 3.3 and results from the trend analysis of the power plants in Sec. 3.4.

## 2. Methods

### 2.1. OMI retrievals

The Ozone Monitoring Instrument (OMI) was launched on NASA's Aura satellite in July 2004 and has been providing measurements of ultraviolet and visible radiation with a spatial resolution of up to 13 km by 24 km (Levelt et al., 2006). We will use  $\text{NO}_2$  column data derived from OMI measurements from 3 different sources. The first is the Berkeley High Resolution  $\text{NO}_2$  product (BEHR v2.0a, Russell et al. (2011)). The second is the DOMINO v2.0 product (Boersma et al., 2007, 2011). The third is the NASA OMI  $\text{NO}_2$  v2.1 product (Bucsele et al., 2013; Lamsal et al., 2014). Note that the BEHR product has higher resolution inputs, particularly for the vertical profile, which will give a systematically different decay profile downwind of point sources.

For each product, we take the level 2 swath data and oversample it onto 4 km grids that are centered on the source of interest as described in de Foy et al. (2014, 2009). Oversampling takes data at a variable pixel resolution and interpolates them to a grid with finer pixels. When taking averages over extended time periods, a high resolution picture of individual plumes can be obtained in this way. Note that by oversampling to a fine grid, the method accounts for the varying area of the data pixels. Although Lee et al. (2011b) recommend weighting the OMI values with the inverse area of the swath pixel to give a higher weight to the near-nadir data, this was not done in the current work. OMI has suffered from a partial blockage of its field of view leading to row anomalies. In order to have a consistent record, we limit the analysis to rows 10 to 27 for the years from 2005 to 2011 inclusive. For all 3 retrievals we use the QA flag to exclude questionable data points. Furthermore, we exclude all points with a cloud fraction exceeding 20%.

Finally, all  $\text{NO}_2$  fields are scaled by an assumed  $\text{NO}_x$  to  $\text{NO}_2$  ratio of 1.32 (Beirle et al., 2011). This ratio depends on a number of factors including altitude, photolysis and ozone concentration. Using a single value increases the uncertainty in the results, which could be reduced by using photochemical grid model results to estimate site-specific ratios in future work. All emissions are reported in metric tonnes of  $\text{NO}_2$  equivalent emissions per year.

## 2.2. Continuous Emissions Monitoring System and meteorological data

NO<sub>x</sub> emissions of major power plants are measured by the Continuous Emissions Monitoring System (CEMS) and were obtained through the US-EPA's Technology Transfer Network. We used monthly averaged data matched to each available OMI scene. For the evaluation, the estimated emissions were compared with the average of the emissions for all the scenes included in the analysis. Note that we also performed the analysis by using daily averaged CEMS data, and this gave the same results as using the monthly averages. We also analyzed hourly data for the power plants which showed that they are mostly baseline power plants with either no or very limited diurnal variations in emissions. We therefore decided to stay with monthly averages as this is simpler than using the daily data.

Power plants for the study were selected if they accounted for more than 90% of the emissions in their 0.4° grid box according to the Emission Database for Global Atmospheric Research version 4 (EDGAR). In addition, we excluded power plants that were too close to urban areas or other sources as the Exponentially-Modified Gaussian method requires a clear separation between different sources. Overall, we had a list of 29 power plants of which 19 are in common with Duncan et al. (2013). One of these is a merger of Four Corners and San Juan power plants in New Mexico as they are close enough to each other and hence can be treated as a single source. While no site is perfectly isolated from other sources, these power plants were deemed to be sufficiently separated from surrounding sources to allow for a robust estimate of the power plant emissions. Table 1 lists the facilities along with their location and the annualized emissions during the 2005 to 2011 interval for the ozone season

(May to September) and for the rest of the year (October to April). Fig. 1 shows the location of the power plants on a map of the USA.

The equations for the emissions estimates described below (Secs. 2.3 and 2.4) are a linear function of the wind speed. The EMG method also requires that plumes be rotated to have a uniform flow direction (Valin et al., 2013; de Foy et al., 2014). Wind measurements are therefore a crucial part of the method. We tested data from both the North American Regional Reanalysis project (NARR, Mesinger et al. (2006)) and from the European Centre for Medium-Range Weather Forecasts's ERA-Interim reanalysis (Dee et al., 2011). For NARR, we found that the best estimates were obtained using the average wind speeds for the 15 hPa layer above the surface. For ERA-Interim we used the 10-m surface wind speeds. Compared with NARR, using ERA-Interim winds gave emissions estimates that were slightly closer to the CEMS data and so all the results presented in this paper will use ERA-Interim winds. Overall, the difference between the 2 was minor as can be seen by comparing the results presented in the main paper with the tables and figures using the NARR data which are in the supplementary material.

## 2.3. Exponentially-Modified Gaussian fit

The Exponentially-Modified Gaussian fit has been used to estimate emissions of isolated sources along with estimates of the chemical lifetime (Beirle et al., 2011). The line densities obtained from the cross-wind integration of column densities are used as input to a fit of a first-order reacting Gaussian plume. This requires that all the plumes are transported in the same direction, and so we rotate all the OMI swath data as recommended by Valin et al. (2013). This was done using the ERA-Interim surface winds as discussed in Sec. 2.2 above.

**Table 1**

Location of the power plants included in the study along with emissions from the Continuous Emissions Monitoring System (CEMS) outside the ozone season (Oct–Apr) and during the ozone season (May–Sep). Annual trends of emissions during the ozone season are shown for 2005 to 2011 for the CEMS data as well as for the box model estimates of emissions using three different OMI data products.

Site	Location		CEMS emissions		Ozone season trends			
	Lat	Lon	Oct–Apr	May–Sep	CEMS	BEHR	DOMINO	OMI NO <sub>2</sub> v2.1
	deg N	deg E	kt/yr	kt/yr	kt/yr/yr	kt/yr/yr	kt/yr/yr	kt/yr/yr
Crystal River, FL	28.96	–82.70	24.36	27.51	–5.94	–3.93	–2.88	–1.29
Barry, AL	31.01	–88.01	11.96	13.21	–2.23	–1.53	–1.77	–2.24
E.C. Gaston, AL	33.24	–86.46	19.64	15.98	–1.02	–1.44	–1.28	–1.21
Belews Creek, NC	36.28	–80.06	11.63	3.67	–0.24	–0.28	–0.04	0.15
Paradise, KY	37.26	–86.98	38.33	9.12	0.63	1.11	0.77	0.55
White Bluff, AR	34.42	–92.14	14.08	16.93	0.35	0.18	–0.23	–0.18
Independence, AR	35.67	–91.41	13.61	16.13	–0.24	–0.44	–0.46	–0.20
New Madrid, MO	36.51	–89.56	23.09	5.64	–0.77	–0.88	–0.84	–0.79
T. Hill Energy Center, MO	39.55	–92.64	11.95	10.97	–1.50	–1.80	–1.36	–1.15
Kincaid, IL	39.59	–89.50	20.14	3.69	0.86	1.20	0.89	0.56
Powerton, IL	40.54	–89.68	26.74	15.75	–0.84	–0.72	–1.33	–1.43
Jeffrey Energy Center, KS	39.28	–96.12	21.39	21.56	–2.68	–0.37	–0.36	0.01
George Neal North, IA	42.30	–96.36	10.01	9.89	–0.72	–0.47	–1.12	–0.37
Sooner, OK	36.45	–97.05	11.15	12.32	–0.53	–0.50	–0.61	–0.20
Martin Lake, TX	32.26	–94.57	14.84	17.11	–0.12	–1.31	–1.00	–0.61
Harrington Station, TX	35.30	–101.75	9.23	9.76	–1.40	–0.96	–1.02	–0.48
Monticello, TX	33.09	–95.04	12.55	12.45	–0.79	–0.88	–0.80	–0.68
Gerald Gentleman St., NE	41.08	–101.14	16.58	14.69	–1.46	–1.73	–1.69	–1.10
Laramie, WY	42.11	–104.88	18.90	16.72	–1.26	–1.13	–1.52	–0.91
Milton R. Young, ND	47.07	–101.21	17.03	17.41	–2.18	–0.90	–1.23	–0.76
Colstrip, MT	45.88	–106.61	27.67	22.97	–3.84	–3.02	–3.32	–2.36
Jim Bridger, WY	41.74	–108.79	23.15	21.80	–3.21	–2.24	–2.32	–3.01
Dave Johnston, WY	42.84	–105.78	11.96	11.53	–1.43	–0.77	–1.08	–1.14
Craig, CO	40.46	–107.59	15.91	16.07	–0.86	–1.08	–1.14	–0.53
Hunter, UT	39.17	–111.03	17.79	17.48	–0.64	–1.62	–1.87	–1.99
Intermountain, UT	39.51	–112.58	25.51	28.06	–0.26	0.36	0.66	0.14
Navajo, AZ	36.90	–111.39	28.96	32.64	–2.39	–2.71	–2.47	–2.49
Coronado, AZ	34.58	–109.27	12.83	13.23	–0.75	–0.26	–0.26	–0.38
Four Corners + San Juan, NM	36.75	–108.46	60.64	66.03	–2.67	–3.78	–3.98	–3.66

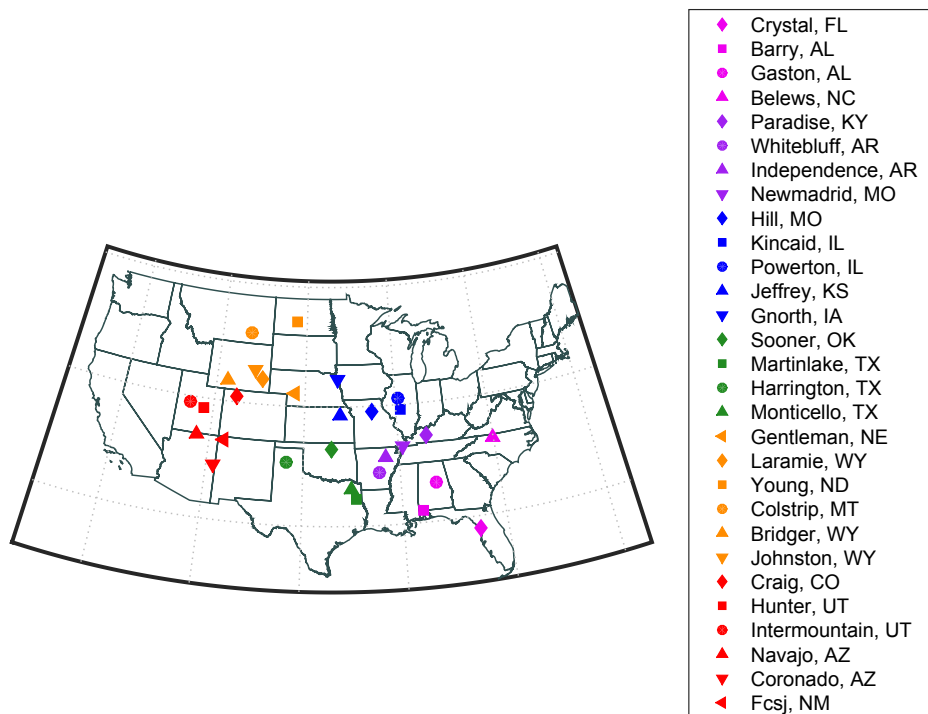


Fig. 1. Map showing the location of the power plants used in this study. Each power plant has a symbol colored by geography which will be used throughout the paper.

The derivation of the equations is described in more detail in de Foy et al. (2014) and yields the following equation for the expected plume fit:

$$L_{fit}(x) = \frac{a}{2} \exp\left(\frac{\sigma_x^2}{2x_0^2} - \frac{x - \mu_x}{x_0}\right) \left(1 - \operatorname{erf}\left(\frac{\sigma_x^2 - x_0(x - \mu_x)}{\sqrt{2}\sigma_x x_0}\right)\right) + Bkg \quad (1)$$

Where  $a$  is the amount of mass  $M$  in the plume over the interval  $x_0$ , the smoothing length scale is given by  $\sigma_x$  and the length scale for chemical decay is  $x_0$ . The optimal plume location along the  $x$  axis is given by  $\mu_x$ , and the background value is given by  $Bkg$ .

From this equation, we can use a representative plume transport speed  $U$  to convert length scales to time scales, and hence we can obtain the emission rate and the lifetime as follows:

$$E = Ua \quad (2)$$

$$\tau_m = \frac{x_0}{U} \quad (3)$$

In practice, de Foy et al. (2014) found that the estimate of emissions is accurate, but that the lifetime estimate is not a reliable measure of the chemical lifetime because it is influenced by plume meandering as well as by grid resolution and sampling issues. We therefore call it the mixed lifetime  $\tau_m$ , which we take to be a combination of the chemical lifetime  $\tau_c$  and a separate lifetime  $\tau_a$  that accounts for the approximations made between the real case and the theoretical relation.

In practice, we use the optimization routine “fmincon” in MATLAB to determine an optimal set of parameters based on the line densities from OMI column densities described in Sec. 2.1. Constraints in the routine are used to prevent unphysical negative values for  $a$ ,  $x_0$ ,  $\sigma_x$ , and  $Bkg$ .

#### 2.4. Box model

As described in de Foy et al. (2014), the simplest method for evaluating emissions from column densities is to use a box model that includes the source of interest. For this method, we use a single value of average column density defined over a specified box size, and therefore we can derive a single parameter of emissions strength. The chemical lifetime needs to be included as an input into the model. The emissions ( $E$ ) can be obtained from the following equation:

$$E = \frac{M - M_{Bkg}}{\tau} \quad (4)$$

Where  $M$  is the mass of substance in the box and  $M_{Bkg}$  is the background amount which ideally includes all the mass of substance that is not part of the plume.  $\tau$  is the residence time of the substance in the box, and is determined by the combination of the dispersion time  $\tau_d$  and a mixed lifetime  $\tau_m$ . As described for the EMG method above,  $\tau_m$  is a combination of the chemical lifetime  $\tau_c$  and a separate lifetime  $\tau_a$  that accounts for approximations in the method. These include factors that influence measurements of dispersion such as plume meandering and grid resolution issues.

$$\frac{1}{\tau} = \frac{1}{\tau_d} + \frac{1}{\tau_c} + \frac{1}{\tau_a} \quad (5)$$

The dispersion lifetime can be estimated by considering a source that is in the middle of a box of dimensions  $\Delta x$  by  $\Delta y$ :

$$\tau_d = \frac{\Delta x}{2U} \quad (6)$$

Where  $U$  is the speed of the plume in the box.

With the box model method, we cannot determine the chemical reaction time from the model. Lamsal et al. (2010) estimated a  $\text{NO}_x$  chemical lifetime varying between 7 h in the summer and 17 h in

the winter over the eastern United States. This was done using data from 2005 at a resolution of  $0.1^\circ$ , and was based on comparing the actual column measurement and effective emissions in the data with simulated columns from a photochemical model. These lifetime estimates are similar to the ones for Riyadh given by Valin et al. (2013) using data at a resolution of 4 km. Note however that there remains considerable uncertainty in these estimates. For example, existing studies cited in Lamsal et al. (2010) report summer  $\text{NO}_x$  lifetimes in power plant plumes ranging from 1.5 to 6.4 h.

In this study, we know the emissions from the power plants, and so we can test which estimates of the mixed lifetime give the results with the highest accuracy, as will be discussed in Sec. 2.4. The sensitivity tests found that the best estimates were obtained with a chemical lifetime of 7 h and an approximations lifetime of 3 h, which corresponds to a mixed lifetime of 2 h.

### 2.5. Uncertainty analysis

We use the bootstrapping algorithm to estimate the uncertainties in the results. Each estimation is based on a grid of average column densities based on multiple satellite scenes. For the uncertainty calculation, we perform 100 estimates where we select the scenes at random with replacement. In this way, we account for uncertainties due to individual retrieval errors as well as uncertainties due to different plume transport or meteorological conditions on each day of the retrieval. Based on the 100 bootstrap estimates, we obtain the interquartile range which will be displayed below. We will also report the coefficient of variation of the results by dividing the standard deviation of the bootstrap estimates by the mean. When expressed as a percentage, this gives a measure of the relative uncertainty in the results since it represents a standardized measure of the dispersion of the probability distribution of the estimates.

Results will be shown for both the complete set of stations and time intervals, as well as for subsets that exclude outliers. This is because some of the methods and time intervals lead to a few extreme outliers that dominate the statistical metrics. The outliers are identified using the Iteratively Reweighted Least Squares (IRLS) procedure. A least squares fit is applied to the data and the residual is calculated for each point in the fit. If the residual of a particular data point is greater than 2 times the standard deviation of all the residuals, then that point is deemed an outlier and excluded by the IRLS procedure.

## 3. Results & discussion

### 3.1. Exponentially-Modified Gaussian results

We perform the fits for the ozone season (May to September) for all years together, and then separately for each individual ozone season. The EMG method is performed on a domain that is 100 km by 100 km, which means that it includes 25 by 25 grid cells with a resolution of 4 km each. We found that this domain size gave a sufficient number of data points for fitting a smooth EMG profile while minimizing contamination from surrounding sources. We further note that the EMG results were robust with respect to the length scale chosen. The ozone season contains 153 days. Depending on the site location and the year, there are between 31 and 56 scenes with valid data for each ozone season. The annual average varies between 35 for the Crystal River power plant and 49 for the Intermountain power plant. Within each scene, the percentage of valid pixels varies from a minimum of 44% to a maximum of 92% depending on the site and year. On average there is valid data for 63% of the valid scene, which corresponds to an average of 26 valid data points for each grid point during the length

of an ozone season. These numbers are low compared to the 153 days in the time period due to the reduced number of rows being used (rows 10–27) and the extensive screening by data quality flag and by cloud fraction.

Fig. 2 shows the EMG fit for the Crystal River power plant in Florida using an average of all the OMI scenes for May to September from 2005 to 2011 inclusive. The numerical fit follows the data very closely. The estimated emissions for this example are 21.5 kt/yr, which are biased low compared to the CEMS value of 27.6 kt/yr. The estimated mixed lifetime is 3.9 h, which is much shorter than the expected chemical lifetime of around 7 h (Lamsal et al., 2010).

Fig. 3 shows the emissions estimates from the EMG method versus the CEMS data for each power plant in the study. Pearson's correlation coefficient squared ( $r^2$ ) of the estimated vs. the measured emissions for all power plants is 0.19. Excluding the 3 power plants with the greatest discrepancy increases  $r^2$  to 0.73. Table 2 shows further statistics on the performance of the method for the cases using data averaged over the 7 ozone seasons. The averaged emissions over the 7 ozone seasons are listed for each power plant in Table S1 in the supplementary material.

The uncertainty in the results was estimated by the bootstrap algorithm, as described in Sec. 2.5. These uncertainties are calculated by selecting different scenes of satellite data for inclusion in the analysis. Each scene will have associated with it both measurement errors and numerical errors. The numerical errors are due to different levels of discrepancy between the assumptions required by the estimation method and the real case. If we assume that both types of errors are randomly distributed from scene to scene, then selecting scenes at random yields an estimate of the impact of all of these errors on the parameter. The interquartile ranges of the estimates in Fig. 3 show clearly that the power plants with high over-estimates of the emissions are also the ones with large uncertainties. The coefficients of variation of the estimates, which is a measure of the relative uncertainty, vary from 6.4% to 145%, with a mean of 58%. This shows that the uncertainties in the EMG emission estimates are considerable.

Fig. 4 shows the mixed lifetime estimated by the EMG method. The longest lifetime is 4 h for the combined Four Corners and San Juan power plants in New Mexico. Some of the plumes have estimated mixed lifetimes that are shorter than 30 min (Kincaid, IL and Paradise, KY). Note however that these are smaller sources, especially during the ozone season. It is therefore possible that the lifetime is short because satellite-retrieved columns surrounding the source are close to the detection threshold. Overall, this

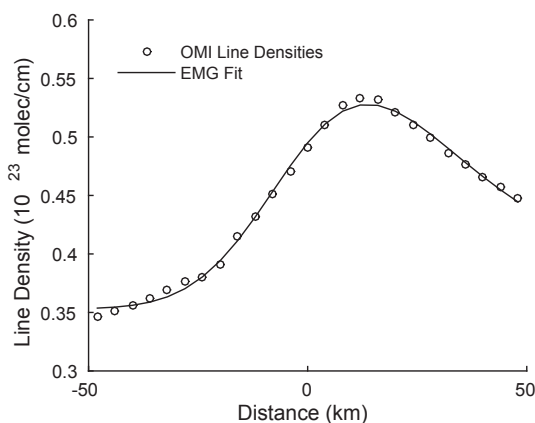
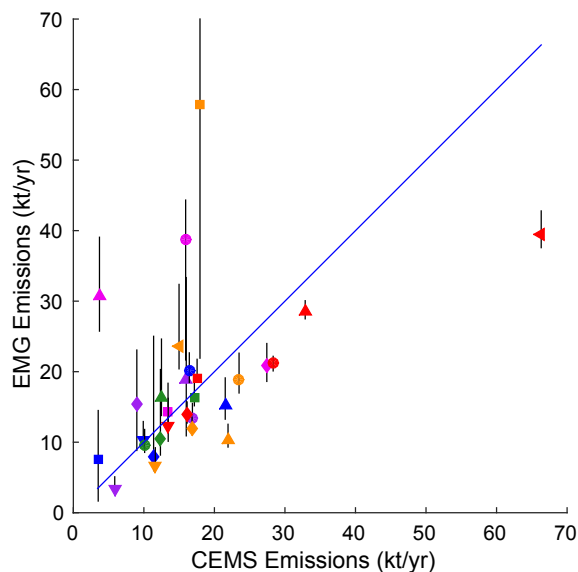


Fig. 2. OMI BEHR  $\text{NO}_2$  line density and Exponentially-Modified Gaussian fit for Crystal River power plant, Florida using the average column densities of the ozone seasons (May–Sep) from 2005 to 2011.



**Fig. 3.** Emissions estimates from the Exponentially-Modified Gaussian method versus the CEMS data for each power plant. The uncertainty of the estimates is shown by the vertical bars which are based on the interquartile range obtained from 100 bootstrapped estimates of the emissions. See Fig. 1 for legend.

confirms the findings in de Foy et al. (2014) that lifetimes estimated by the method are biased low and cannot be used as reliable estimates of the true chemical lifetime. It is also consistent with the short lifetimes suggested by comparing the box model results with

**Table 2**

Statistical metrics for the comparison of emissions estimates from different methods with CEMS data. Results shown for both the Exponentially-Modified Gaussian (EMG) method and the box model method. “7 year” shows results using a single average of column densities over all ozone season months from 2005 to 2011. “1 year” shows results using averaged column densities for each ozone season. “2 month” uses averages over 2 month periods covering 2005 to 2011 (42 intervals in the time series). Statistics are calculated with the complete data set (“All”) as well as with outliers excluded by the Iteratively Reweighted Least Squares (IRLS) method, as described in the text.

	IRLS	No. Obs #	$r^2$	CEMS kt/yr	Estimate kt/yr	Bias kt/yr	RMSE kt/yr
<b>BEHR</b>							
EMG 7 year	All	29	0.19	17.28	18.72	1.43	12.28
	IRLS	26	0.73	17.85	15.83	-2.02	6.90
Box 7 year	All	29	0.88	17.28	17.46	0.18	4.15
	IRLS	27	0.91	17.77	18.57	0.81	3.66
Box 1 year	All	203	0.84	17.25	17.11	-0.15	5.13
	IRLS	194	0.87	16.89	16.54	-0.35	4.42
Box 2 month	All	1218	0.49	18.70	17.04	-1.66	10.91
	IRLS	1146	0.63	17.80	16.13	-1.66	8.01
<b>DOMINO</b>							
EMG 7 year	All	29	0.03	17.30	17.88	0.58	18.80
	IRLS	27	0.54	17.75	13.67	-4.08	8.93
Box 7 year	All	29	0.80	17.30	14.71	-2.59	5.97
	IRLS	27	0.84	16.52	13.99	-2.53	5.30
Box 1 year	All	203	0.77	17.27	14.44	-2.83	6.73
	IRLS	190	0.85	16.63	13.66	-2.96	5.73
Box 2 month	All	1215	0.34	18.69	17.65	-1.04	15.82
	IRLS	1158	0.52	18.15	15.74	-2.41	10.44
<b>OMI NO<sub>2</sub> v2.1</b>							
EMG 7 year	All	29	0.04	17.27	22.11	4.85	20.15
	IRLS	27	0.11	17.28	18.20	0.92	13.67
Box 7 year	All	29	0.81	17.27	13.09	-4.17	6.50
	IRLS	28	0.85	16.92	13.21	-3.71	5.77
Box 1 year	All	203	0.77	17.28	12.95	-4.33	7.37
	IRLS	193	0.85	16.75	12.85	-3.90	6.14
Box 2 month	All	1218	0.46	18.73	14.73	-4.00	11.82
	IRLS	1162	0.58	17.89	13.66	-4.24	9.43

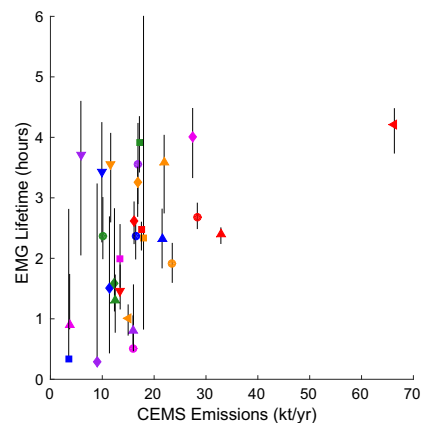


**Fig. 4.** Lifetime estimates from the Exponentially-Modified Gaussian method for each power plant ( $\tau_m$ , Eq. (3)), plotted against CEMS emissions. Vertical bars show the interquartile range of the bootstrapped estimates, which represent the uncertainty range. See Fig. 1 for legend.

the known emissions, as will be described in Sec. 3.2. The uncertainty bars on the lifetimes are much larger than the ones for the emissions estimates. On average, the uncertainty of the estimates, given by the coefficient of variation, is 100% which further indicates that these estimates should be treated with caution.

When we perform the analysis for individual ozone seasons (May–Sep) by year, we have 7 data points for each ozone season from 2005 to 2011. We find that the performance of the EMG method drops significantly, with an overall  $r^2$  of 0.02. This is due to many cases of large over-estimates of the emissions. We conclude from this that on shorter time periods there is insufficient data to provide a smooth profile in order to obtain an accurate fit. As reported above, for the time interval of a single ozone season there are only 35 scenes per estimate, and of those there is only 65% data availability which means that any pixel in the grid will have only 26 valid data points.

### 3.2. Box model results

Fig. 5 shows the average column densities for all ozone seasons from 2005 to 2011 for the Crystal River power plant. Note that we use rotated swath data which give the distinct eastward direction of the plume. Although the plume rotation is not necessary for the box model method, it does lead to improved estimates of the background value compared with using unrotated swath data, and hence to more reliable results.

A critical component of the box model method is the estimation of  $M$  and  $M_{Bkg}$  in Eq. (4). We have found that we obtain optimal results when we calculate  $M_{Bkg}$  from the median column density of the oversampled 4 km resolution grids within a box that is 200 km by 200 km. This gives emissions estimates that are not strongly influenced by the size of the box used for the calculation of  $M$ . It is also consistent with using the background level that is calculated by the EMG procedure. When the background is correctly identified, the results are not as sensitive to the definition of  $M$ . In our case, we base the calculation of  $M$  on the average column density of the oversampled 4 km resolution grids in a box that is 50 km by 50 km.

Fig. 6 shows the estimated emissions from the box model versus the CEMS emissions. We present results for all the ozone seasons together, for each ozone season separately, and finally for estimates of the emissions at two month intervals. We use an estimate of  $\tau_m$  of 2 h for calculating the emissions, based on the sensitivity tests described at the end of this section. Estimates of the emissions of

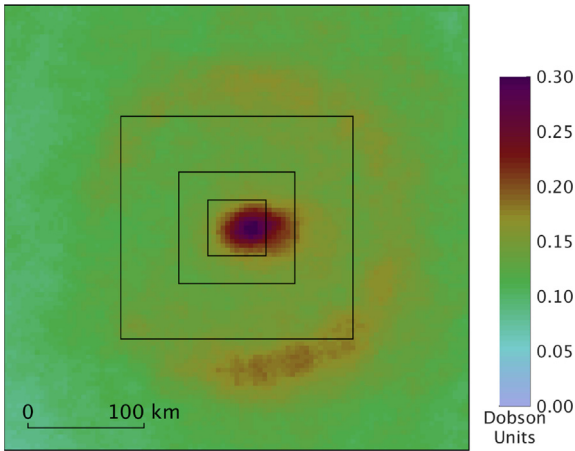


**Fig. 5.** OMI BEHR NO<sub>2</sub> column densities oversampled to 4 km grid for Crystal River power plant rotated using ERA-Interim winds to have eastward plumes. Also shown are the 200 km box used to calculate the background value, the 100 km box used for the EMG method and the 50 km box used to calculate the box model emissions estimate.

the 7 year time period are in excellent agreement with the CEMS data with  $r^2$  of 0.88. Further metrics are presented in Table 2. The estimates continue to be accurate for the individual ozone seasons, as can be seen with an  $r^2$  of 0.84 for the comparison with the CEMS data. We also present results for estimates of emissions at 2 monthly intervals for the complete year, which means there are a maximum of 42 estimated data points over the 7 year period. With this resolution, there is an increase in the scatter of the data and a decrease in  $r^2$  to 0.49.

As described in Sec. 2.5, the uncertainties in the estimates are obtained as coefficients of variation based on 100 realizations of the estimates using the bootstrapping algorithm. Fig. 6 shows that the interquartile range of the bootstrapped emissions estimates are very narrow for the 7 year period, indicating that the results are very robust to the individual days included in the analysis. The corresponding uncertainties are mostly in the range of 4%–10%. For the individual ozone season estimates, the interquartile ranges are larger than for the single 7 year estimate, but are still quite low, especially compared with the uncertainty in the EMG estimates. The coefficients of variation for the ozone season estimates are correspondingly larger, with a median value of 17%.

We next evaluate the accuracy of the time series of emissions estimates versus the CEMS data for each power plant. We do this by

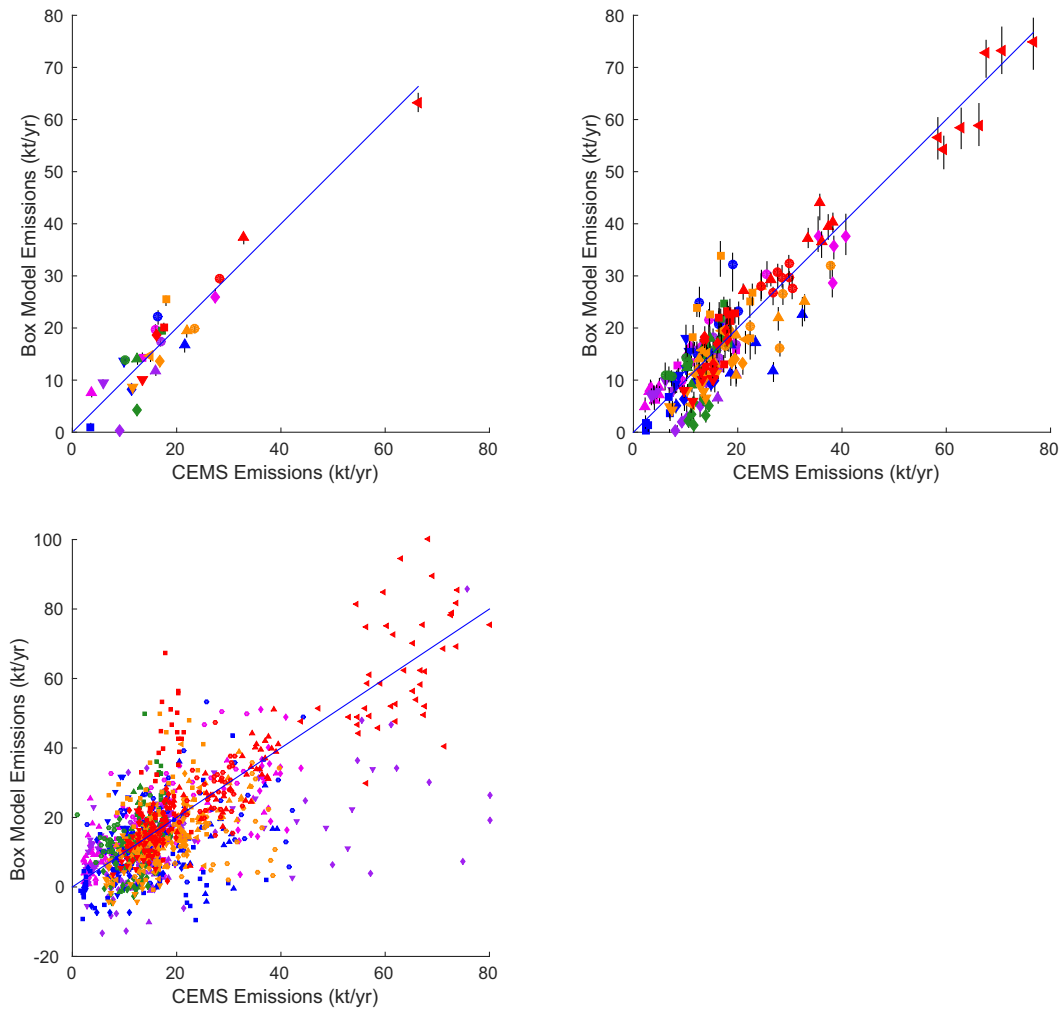


**Fig. 6.** Emissions estimates from the box model method using the OMI BEHR product versus the CEMS data for each power plant. Top left: 7 year average emissions (2005–2011), Top right: individual ozone season emissions (7 years), and Bottom Left: bimonthly emissions. Uncertainty shown for the longer time averages as vertical bars of the interquartile range of 100 bootstrapped estimates. See Fig. 1 for legend.

calculating Pearson's correlation coefficient squared ( $r^2$ ) between the emissions estimates and the CEMS data for the 7 ozone seasons as well as for the 42 bimonthly estimates. The  $r^2$  are plotted against the variability in the CEMS data which is measured by dividing the standard deviation of the emissions with the mean emissions for the 7 or 24 data points. This yields a coefficient of variation as described in Sec. 2.5, except that here it is used to yield a measure of the variability in the emissions themselves, rather than an estimate of the uncertainty.

Fig. 7 shows the  $r^2$  values for the 7 ozone season estimates as well as for the 42 bimonthly estimates as a function of the variability in emissions for each power plant. For the ozone season estimates, the mean  $r^2$  is 0.56, and 14 of the sites have  $r^2$  above 0.7. These are the ones that also tend to have more variation in their emissions. When the CEMS data varies by more than 40% (coefficients of variation above 0.4), all estimates are more accurate. This is to be expected as large variations should be easy to spot in the data and stand out more clearly above the noise in the signal. The box model results do not estimate the variability of the emissions as accurately when the variability is lower than around 40%, with  $r^2$  values dropping to nearly zero in some cases.

For the bimonthly estimates, the mean of the  $r^2$  between the box model estimates and the CEMS data is 0.28. None of the sites have an  $r^2$  above 0.7 and even some of the ones with a high coefficient of variation in the emissions have low correlation coefficients between the estimates and the CEMS data. Overall, we show that the box model estimates can do a good job identifying annual variations but would struggle to correctly capture variations on shorter time scales.

Given that we have a reliable estimate of the true emissions, we can use this information to determine the mixed lifetime  $\tau_m$  that would give a perfect emissions estimate for the estimate of the average emissions of the 7 ozone seasons combined. This is shown in Fig. 8 for each power plant. From this, it can be seen that many of the sites have  $\tau_m$  around 2 h, but that there are sites with both shorter and longer lifetime estimates. The uncertainty bars from the bootstrap method are short for the short lifetimes but much larger for the longer lifetime. Note that this is partly because the scaling factor on the emissions is proportional to the inverse of the lifetime. We did not find a pattern in the lifetimes based on wind speed, latitude, emissions or other characteristics. We also repeated the analysis separately with winter months versus summer months. It would have been reasonable to expect longer lifetimes during the winter, but the comparison did not yield a clear signal one way or the other.

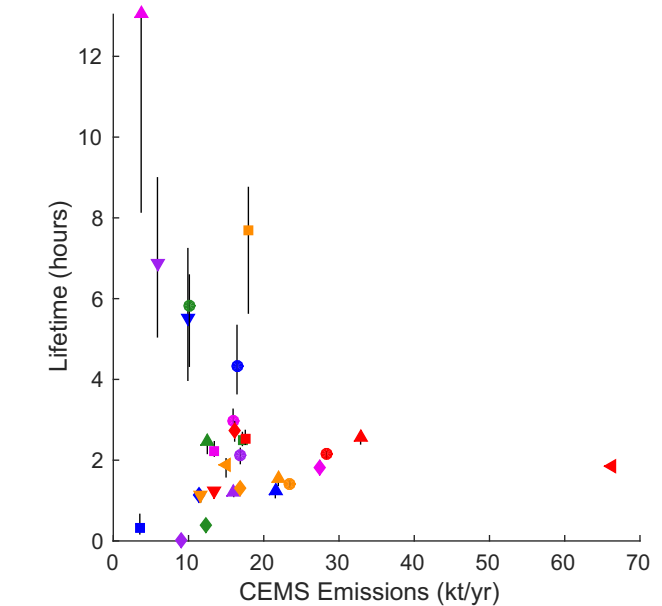
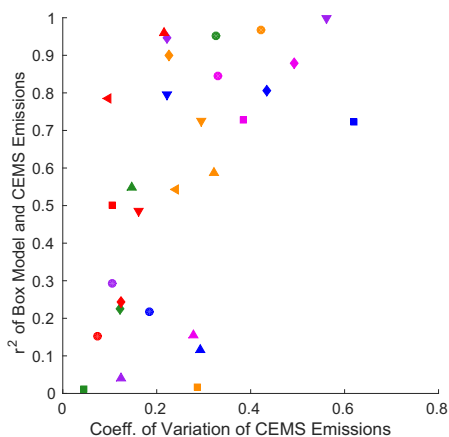


Fig. 8. Lifetime that would give a perfect match of the box model estimated emissions with the CEMS data for the 7-year ozone season averages. This is the mixed lifetime ( $\tau_m$ ) which is the sum of the chemical and the approximations lifetimes. Points plotted against CEMS emissions for each power plant, with vertical bars showing the interquartile range of 100 bootstrapped estimates. See Fig. 1 for legend.

The equations for the box model estimates (Eq. (4)) and for the EMG estimates (Eq. (1)) rely on assumptions of perfect sampling and uniform plume transport. In practice, these assumptions are violated for example because of variable swath resolution; plume meandering; and vertical variation in retrieval sensitivity and plume transport. The results suggest that these discrepancies lead to a lifetime term representing approximations in the equation ( $\tau_a$ ) of around 3 h which precludes the derivation of chemical lifetime of the data in their current form. Assuming that the chemical lifetime of  $\text{NO}_x$ ,  $\tau_c$  is around 7 h, this gives a mixed lifetime,  $\tau_m$ , of 2 h for use in the calculation. Future satellite instruments will have finer sampling resolutions and more frequent temporal resolutions which will help to go past this barrier.

### 3.3. Comparison of different data products

There are two main products of tropospheric column  $\text{NO}_2$  based on the OMI data: DOMINO and the NASA OMI v2.1 products. Also

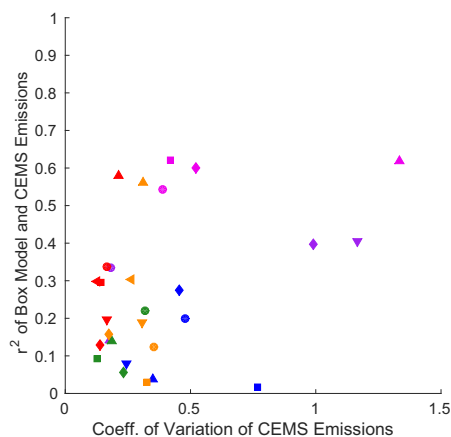


Fig. 7. Correlation coefficient squared ( $r^2$ ) of box model emissions with CEMS data for annual estimates (left, 7 data points per time series) and bimonthly estimates (right, 42 data points per time series) for each power plant. See Fig. 1 for legend.

available is the BEHR regional product based on NASA OMI v2.1 and high-resolution albedo information from MODIS. We performed the analysis that has been presented so far in this paper with all three products to evaluate the sensitivity of the results to product choice, and to evaluate the differences due to the different products. As a caveat, we should say that the estimation methods were developed while working with the BEHR product, so that this has an advantage over the other ones in the comparisons. We show results using all the data points as well as using a subset that excludes the outliers using the IRLS procedure. This is particularly important for the EMG results which tend to suffer from extreme values.

Table 2 shows results for the three data products for the following metrics:  $r^2$ , the mean emissions, the bias, the Root Mean Square Error (RMSE) and the number of observations used in each comparison. This shows that even though the highest correlation coefficients are obtained with the BEHR data product the other two products are not far behind. In particular, the correlation coefficients of the OMI NO<sub>2</sub> v2.1 product are closer to those of the BEHR product than the DOMINO coefficients. The mean emissions estimates are close to the CEMS data, with the lowest bias for BEHR. The normalized bias is lower than 10% for all the estimates using BEHR. There is a more significant negative bias for DOMINO estimates reaching -20%, and even more so for the OMI NO<sub>2</sub> v2.1 product reaching -25% for the box model results. In keeping with the previous discussion, the RMSE errors are comparable with the lowest values for the BEHR product and the highest for DOMINO and OMI NO<sub>2</sub> v2.1.

#### 3.4. Emission trends

One of the main applications of satellite remote sensing of air pollution is detecting trends in emissions. We use a least squares fit of the emissions of the 7 separate ozone seasons to estimate the linear trends of the emissions in the CEMS data and in the box model estimates. Fig. 9 shows the annualized change in emissions in the satellite estimates versus those in the CEMS data as well as the percentage change over the 7 year period using the BEHR product. The data are shown in Table 1 for all 3 satellite retrieval products. The trends in the CEMS data vary from a minimum change per year of -5.9 kt/yr at Crystal River to a maximum of 0.9 kt/yr at Kincaid. There is an  $r^2$  of 0.75 for the comparison of the box model estimates with the CEMS data. Over the 7 year period, the average percentage reduction among the 27 sites varied from a

79% reduction to a 13% increase in the CEMS data, and from an 81% reduction to an 8% increase in the box model estimate. The average reduction was 38% in the CEMS data and 35% in the box model data (Note that Kincaid, IL and Paradise, KY had increases based on very low initial emissions in the box model estimates, and so they were excluded from the percentage calculations). This shows that the trend calculation is more sensitive to errors than the emissions estimates themselves, but that overall the satellite data yield a useful estimate of emission trends. As before, the trends calculated using the BEHR product were the closest to the trends in the CEMS data, but both the DOMINO and the OMI NO<sub>2</sub> v2.1 products gave reliable results.

#### 4. Summary

We have evaluated the emissions estimates obtained from the Exponentially-Modified Gaussian method and from the box model method. In the process, we identified the need for reliable wind speed estimates and found that ERA-Interim surface winds gave the best estimates followed by layer-averaged winds from NARR in the 15 hPa above the surface. The box model estimates were sensitive to the method used for determining the background value, the size of the box used for calculating the average column density over the plume, and the lifetime used in the calculation. We found that using the median column density in an area 200 km by 200 km gave the best background estimates, and that using the average column density in an area 50 km by 50 km gave the best emissions estimates. For the lifetime, we introduced a separate lifetime  $\tau_a$  that represents model inaccuracies and that is around 3 h, leading to a mixed lifetime of 2 h which gives emissions estimates with low biases.

Comparisons with CEMS data showed that the EMG method gave reliable estimates over multi-annual averages but not over time spans less than a year. The method was robust with respect to domain choice, but there was a significant uncertainty in the estimates which is a function of the scenes selected in the analysis. In comparison, the box model method yielded emissions estimates that are both more accurate and more robust even though the domains must be selected with care. The box model was able to correctly identify emissions trends on an annual time scale using data during the ozone season, but did not perform as well with 2 month intervals.

The analysis was carried out with the two main OMI data products: DOMINO v2.0 and NASA OMI NO<sub>2</sub> v2.1 as well as with the

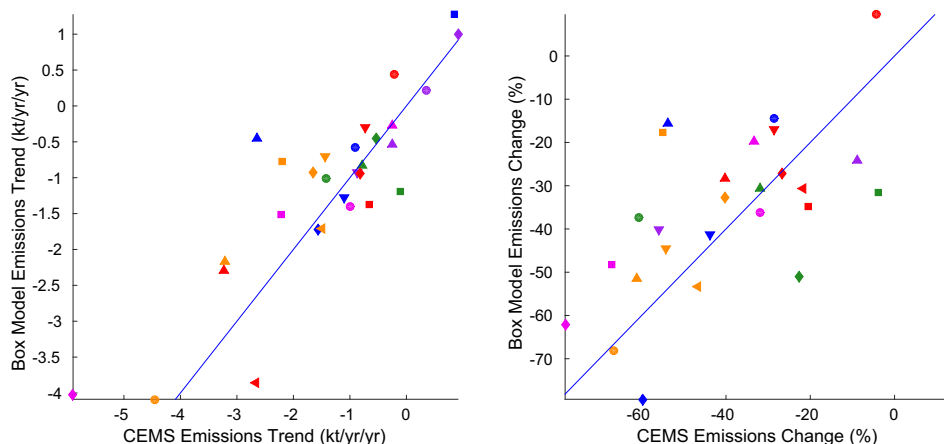


Fig. 9. Trends in emissions in the box model estimates versus trends in the CEMS data calculated with a least squares fit using 7 ozone seasons from 2005 to 2011. Left: changes in kt/yr for each power plant. Right: Overall percentage change over the 7 years (Paradise and Kincaid are off the chart due to low starting emissions). See Fig. 1 for legend.

Berkeley High Resolution regional product (BEHR v2.0a). All three were found to give reliable estimates that were broadly in agreement with each other. Overall the best results were obtained with BEHR first, and OMI NO<sub>2</sub> v2.1 s. Having identified strengths and weaknesses of estimation methods using known sources, this study contributes to the understanding and confidence of emissions estimates using OMI data for sources with no comparable emissions data. It also suggests that improved estimates will be possible with the next generation of satellite instruments being placed in orbit in the coming years.

## Acknowledgments

This research was funded by the NASA Air Quality Applied Sciences Team (AQA) program, NASA grant #NNX11AJ63G, including funding for the AQA Tiger Team “Relationships and trends among satellite NO<sub>2</sub> columns, NO<sub>x</sub> emissions, and air quality in North America.” We are grateful for valuable comments and discussion from the team members and the team leader and assistant leader, Daniel J. Jacob and Tracey Holloway. We thank the anonymous reviewers for their comments which have helped improve the paper.

## Appendix A. Supplementary data

Supplementary data related to this article can be found at <http://dx.doi.org/10.1016/j.atmosenv.2015.05.056>.

## References

- Beirle, S., Boersma, K.F., Platt, U., Lawrence, M.G., Wagner, T., 2011. Megacity emissions and lifetimes of nitrogen oxides probed from space. *Science* 333, 1737–1739.
- Beirle, S., Hörmann, C., Penning de Vries, M., Dörner, S., Kern, C., Wagner, T., 2014. Estimating the volcanic emission rate and atmospheric lifetime of SO<sub>2</sub> from space: a case study for Kilauea volcano, Hawaii. *Atmos. Chem. Phys.* 14, 8309–8322.
- Boersma, K., Eskes, H., Dirksen, R., Veefkind, J., Stammes, P., Huijnen, V., Kleipool, Q., Sneep, M., Claas, J., Leitão, J., Richter, A., Zhou, Y., Brunner, D., 2011. An improved tropospheric NO<sub>2</sub> column retrieval algorithm for the Ozone Monitoring Instrument. *Atmos. Meas. Tech.* 4, 1905–1928.
- Boersma, K., Jacob, D., Bucsel, E., Perring, A., Dirksen, R., van der, A.R., Yantosca, R., Park, R., Wenig, M., Bertram, T., Cohen, R., 2008. Validation of OMI tropospheric NO<sub>2</sub> observations during INTEX-B and application to constrain emissions over the eastern United States and Mexico. *Atmos. Environ.* 42, 4480–4497.
- Boersma, K.F., Eskes, H.J., Veefkind, J.P., Brinkman, E.J., van der, A.R.J., Sneep, M., van den Oord, G.H.J., Levelt, P.F., Stammes, P., Gleason, J.F., Bucsel, E.J., 2007. Near-real time retrieval of tropospheric NO<sub>2</sub> from OMI. *Atmos. Chem. Phys.* 7, 2103–2118.
- Bucsel, E., Krotkov, N., Celarier, E., Lamsal, L., Swartz, W., Bhartia, P., Boersma, K., Veefkind, J., Gleason, J., Pickering, K., 2013. A new stratospheric and tropospheric NO<sub>2</sub> retrieval algorithm for nadir-viewing satellite instruments: applications to OMI. *Atmos. Meas. Tech.* 6, 2607–2626.
- Bucsel, E.J., Perring, A.E., Cohen, R.C., Boersma, K.F., Celarier, E.A., Gleason, J.F., Wenig, M.O., Bertram, T.H., Wooldridge, P.J., Dirksen, R., Veefkind, J.P., 2008. Comparison of tropospheric NO<sub>2</sub> from in situ aircraft measurements with near-real-time and standard product data from OMI. *J. Geophys. Res. Atmos.* 113, D16S31.
- Dee, D.P., Uppala, S.M., Simmons, A.J., Berrisford, P., Poli, P., Kobayashi, S., Andrae, U., Balmaseda, M.A., Balsamo, G., Bauer, P., Bechtold, P., Beljaars, A.C.M., van de Berg, L., Bidlot, J., Bormann, N., Delsol, C., Dragani, R., Fuentes, M., Geer, A.J., Haimberger, L., Healy, S.B., Hersbach, H., Hólm, E.V., Isaksen, I., Kållberg, P., Köhler, M., Matricardi, M., McNally, A.P., Monge-Sanz, B.M., Morcrette, J.J., Park, B.K., Peubey, C., de Rosnay, P., Tavolato, C., Thépaut, J.N., Vitart, F., 2011. The era-interim reanalysis: configuration and performance of the data assimilation system. *Q. J. R. Meteorol. Soc.* 137, 553–597.
- Duncan, B.N., Prados, A.I., Lamsal, L.N., Liu, Y., Streets, D.G., Gupta, P., Hilsenrath, E., Kahn, R.A., Nielsen, J.E., Beyersdorf, A.J., Burton, S.P., Fiore, A.M., Fishman, J., Henze, D.K., Hostetler, C.A., Krotkov, N.A., Lee, P., Lin, M., Pawson, S., Pfister, G., Pickering, K.E., Pierce, R.B., Yoshida, Y., Ziemba, L.D., 2014. Satellite data of atmospheric pollution for U.S. air quality applications: examples of applications, summary of data end-user resources, answers to FAQs, and common mistakes to avoid. *Atmos. Environ.* 94, 647–662.
- Duncan, B.N., Yoshida, Y., de Foy, B., Lamsal, L.N., Streets, D.G., Lu, Z., Pickering, K.E., Krotkov, N.A., 2013. The observed response of Ozone Monitoring Instrument (OMI) NO<sub>2</sub> columns to NO<sub>x</sub> emission controls on power plants in the United States: 2005–2011. *Atmos. Environ.* 81, 102–111.
- Fioletov, V., McLinden, C., Krotkov, N., Moran, M., Yang, K., 2011. Estimation of SO<sub>2</sub> emissions using OMI retrievals. *Geophys. Res. Lett.* 38, L21811.
- Fioletov, V.E., McLinden, C.A., Krotkov, N., Yang, K., Loyola, D.G., Valks, P., Theys, N., Van Roozendaal, M., Nowlan, C.R., Chance, K., Liu, X., Lee, C., Martin, R.V., 2013. Application of OMI, SCIAMACHY, and GOME-2 satellite SO<sub>2</sub> retrievals for detection of large emission sources. *J. Geophys. Res. Atmos.* 118, 11399–11418.
- Fishman, J., Iraci, L.T., Al-Saadi, J., Chance, K., Chavez, F., Chin, M., Coble, P., Davis, C., DiGiacomo, P.M., Edwards, D., Eldering, A., Goes, J., Herman, J., Hu, C., Jacob, D.J., Jordan, C., Kawa, S.R., Key, R., Liu, X., Lohrenz, S., Mannino, A., Natraj, V., Neil, D., Neu, J., Newchurch, M., Pickering, K., Salisbury, J., Sosik, H., Subramaniam, A., Tzortziou, M., Wang, J., Wang, M., 2012. The United States’ next generation of atmospheric composition and coastal ecosystem measurements: NASA’s Geostationary Coastal and Air Pollution Events (GEO-CAPE) mission. *Bull. Am. Met. Soc.* 93, 1547–1566.
- de Foy, B., Krotkov, N.A., Bei, N., Herndon, S.C., Huey, L.G., Martínez, A.P., Ruiz-Suárez, L.G., Wood, E.C., Zavala, M., Molina, L.T., 2009. Hit from both sides: tracking industrial and volcanic plumes in Mexico City with surface measurements and OMI SO<sub>2</sub> retrievals during the MILAGRO field campaign. *Atmos. Chem. Phys.* 9, 9599–9617.
- de Foy, B., Wilkins, J.L., Lu, Z., Streets, D.G., Duncan, B.N., 2014. Model evaluation of methods for estimating surface emissions and chemical lifetimes from satellite data. *Atmos. Environ.* 98, 66–77.
- Ghude, S.D., Kulkarni, S.H., Jena, C., Pfister, G.G., Beig, G., Fadnavis, S., van der, A.R., 2013. Application of satellite observations for identifying regions of dominant sources of nitrogen oxides over the Indian subcontinent. *J. Geophys. Res. Atmos.* 118, 1075–1089.
- Hilsenrath, E., Chance, K., 2013. NASA ups the TEMPO on monitoring air pollution. *Earth Observer* 25, 10–16.
- Hoff, R.M., Christopher, S.A., 2009. Remote sensing of particulate pollution from space: have we reached the promised land? *J. Air Waste Manage. Assoc.* 59, 645–675.
- Ialongo, I., Hakkarainen, J., Hyttinen, N., Jalkanen, J.P., Johansson, L., Boersma, K.F., Krotkov, N., Tamminen, J., 2014. Characterization of OMI tropospheric NO<sub>2</sub> over the Baltic sea region. *Atmos. Chem. Phys.* 14, 7795–7805.
- Jena, C., Ghude, S.D., Blond, N., Beig, G., Chate, D., Fadnavis, S., Van der, A.R., 2014. Estimation of the lifetime of nitrogen oxides over India using SCIAMACHY observations. *Int. J. Remote Sens.* 35, 1244–1252.
- Kim, S.W., Heckel, A., Frost, G., Richter, A., Gleason, J., Burrows, J., McKeen, S., Hsie, E.Y., Granier, C., Trainer, M., 2009. NO<sub>2</sub> columns in the western United States observed from space and simulated by a regional chemistry model and their implications for NO<sub>x</sub> emissions. *J. Geophys. Res. Atmos.* 114, D11301.
- Kim, S.W., Heckel, A., McKeen, S., Frost, G., Hsie, E.Y., Trainer, M., Richter, A., Burrows, J., Peckham, S., Grell, G., 2006. Satellite-observed US power plant NO<sub>x</sub> emission reductions and their impact on air quality. *Geophys. Res. Lett.* 33, L22812.
- Lamsal, L., Martin, R., Van Donkelaar, A., Celarier, E., Bucsel, E., Boersma, K., Dirksen, R., Luo, C., Wang, Y., 2010. Indirect validation of tropospheric nitrogen dioxide retrieved from the OMI satellite instrument: insight into the seasonal variation of nitrogen oxides at northern midlatitudes. *J. Geophys. Res. Atmos.* 115, D05302.
- Lamsal, L.N., Krotkov, N.A., Celarier, E.A., Swartz, W.H., Pickering, K.E., Bucsel, E.J., Gleason, J.F., Martin, R.V., Philip, S., Irie, H., Cede, A., Herman, J., Weinheimer, A., Szykman, J.J., Knepp, T.N., 2014. Evaluation of OMI operational standard NO<sub>2</sub> column retrievals using in situ and surface-based NO<sub>2</sub> observations. *Atmos. Chem. Phys.* 14, 11587–11609.
- Lee, C., Martin, R.V., van Donkelaar, A., Lee, H., Dickerson, R.R., Hains, J.C., Krotkov, N., Richter, A., Vinnikov, K., Schwab, J.J., 2011a. SO<sub>2</sub> emissions and lifetimes: estimates from inverse modeling using in situ and global, space-based (SCIAMACHY and OMI) observations. *J. Geophys. Res. Atmos.* 116, D06304.
- Lee, C.J., Brook, J.R., Evans, G.J., Martin, R.V., Mihele, C., 2011b. Novel application of satellite and in-situ measurements to map surface-level NO<sub>2</sub> in the Great Lakes region. *Atmos. Chem. Phys.* 11, 11761–11775.
- Levelt, P.F., van den Oord, G.H., Dobber, M.R., Malkki, A., Visser, H., de Vries, J., Stammes, P., Lundell, J.O., Saari, H., 2006. The ozone monitoring instrument. *IEEE T. Geosci. Remote Sens.* 44, 1093–1101.
- Lu, Z., Streets, D.G., 2012. Increase in NO<sub>x</sub> emissions from Indian thermal power plants during 1996–2010: unit-based inventories and multisatellite observations. *Environ. Sci. Technol.* 46, 7463–7470.
- Lu, Z., Streets, D.G., de Foy, B., Krotkov, N.A., 2013. Ozone monitoring instrument observations of interannual increases in SO<sub>2</sub> emissions from Indian coal-fired power plants during 2005–2012. *Environ. Sci. Technol.* 47, 13993–14000.
- Martin, R.V., 2008. Satellite remote sensing of surface air quality. *Atmos. Environ.* 42, 7823–7843.
- Martin, R.V., Jacob, D.J., Chance, K., Kurosu, T.P., Palmer, P.I., Evans, M.J., 2003. Global inventory of nitrogen oxide emissions constrained by space-based observations of NO<sub>2</sub> columns. *J. Geophys. Res. Atmos.* 108, 4537–4548.
- Mesinger, F., DiMego, G., Kalnay, E., Mitchell, K., Shafran, P., Ebisuzaki, W., Jovic, D., Woollen, J., Rogers, E., Berbery, E., Ek, M., Fan, Y., Grumbine, R., Higgins, W., Li, H., Lin, Y., Manikin, G., Parrish, D., Shi, W., 2006. North American regional reanalysis. *Bull. A. Met. Soc.* 87, 343–360.
- Mijling, B., van der, A.R.J., 2012. Using daily satellite observations to estimate emissions of short-lived air pollutants on a mesoscale. *J. Geophys. Res. Atmos.* 117, D17302.

- Russell, A., Perring, A., Valin, L., Bucseles, E., Browne, E., Wooldridge, P., Cohen, R., 2011. A high spatial resolution retrieval of NO<sub>2</sub> column densities from OMI: method and evaluation. *Atmos. Chem. Phys.* 11, 8543–8554.
- Russell, A.R., Valin, L.C., Cohen, R.C., 2012. Trends in OMI NO<sub>2</sub> observations over the United States: effects of emission control technology and the economic recession. *Atmos. Chem. Phys.* 12, 12197–12209.
- Schaap, M., Kranenburg, R., Curier, L., Jozwicka, M., Dammers, E., Timmermans, R., 2013. Assessing the sensitivity of the OMI-NO<sub>2</sub> product to emission changes across Europe. *Remote Sens.* 5, 4187–4208.
- Schaub, D., Brunner, D., Boersma, K., Keller, J., Folini, D., Buchmann, B., Berresheim, H., Staehelin, J., 2007. SCIAMACHY tropospheric NO<sub>2</sub> over Switzerland: estimates of NO<sub>x</sub> lifetimes and impact of the complex alpine topography on the retrieval. *Atmos. Chem. Phys.* 7, 5971–5987.
- Stavrakou, T., Müller, J.F., Boersma, K.F., van der A., R.J., Kurokawa, J., Ohara, T., Zhang, Q., 2013. Key chemical NO<sub>x</sub> sink uncertainties and how they influence top-down emissions of nitrogen oxides. *Atmos. Chem. Phys. Disc.* 13, 7871–7929.
- Streets, D.G., Canty, T., Carmichael, G.R., de Foy, B., Dickerson, R.R., Duncan, B.N., Edwards, D.P., Haynes, J.A., Henze, D.K., Houyoux, M.R., Jacob, D.J., Krotkov, N.A., Lamsal, L.N., Liu, Y., Lu, Z., Martin, R.V., Pfister, G.G., Pinder, R.W., Salawitch, R.J., Wecht, K.J., 2013. Emissions estimation from satellite retrievals: a review of current capability. *Atmos. Environ.* 77, 1011–1042.
- Streets, D.G., de Foy, B., Duncan, B.N., Lamsal, L.N., Li, C., Lu, Z., 2014. Using Satellite Observations to Measure Power Plant Emissions and Their Trends. *Environmental Manager (em)* February, pp. 16–21.
- Valin, L., Russell, A., Cohen, R., 2013. Variations of OH radical in an urban plume inferred from NO<sub>2</sub> column measurements. *Geophys. Res. Lett.* 40, 1856–1860.
- Valin, L.C., Russell, A.R., Cohen, R.C., 2014. Chemical feedback effects on the spatial patterns of the NO<sub>x</sub> weekend effect: a sensitivity analysis. *Atmos. Chem. Phys.* 14, 1–9.
- Veefkind, J., Aben, I., McMullan, K., Förster, H., de Vries, J., Otter, G., Claas, J., Eskes, H., de Haan, J., Kleipool, Q., van Weele, M., Hasekamp, O., Hoogeveen, R., Landgraf, J., Snel, R., Tol, P., Ingmann, P., Voors, R., Kruizinga, B., Vink, R., Visser, H., Levelt, P., 2012. TROPOMI on the ESA Sentinel-5 precursor: a GMES mission for global observations of the atmospheric composition for climate, air quality and ozone layer applications. *Remote Sens. Environ.* 120, 70–83 (The Sentinel Missions – New Opportunities for Science).